Electronic Transition and Energy Transfer Processes in $LaPO_4$−Ce^{3+}/Tb^{3+} Nanowires

Lixin Yu, Hongwei Song,* Zhongxin Liu, Linmei Yang, and Shaozhe Lu Zhuhong Zheng

Key Laboratory of Excited-State Physics, Changchun Institute of Optics, Fine Mechanics, and Physics, Chinese Academy of Sciences, 16 Eastern Nan-Hu Road, Changchun 130033, People's Republic of China

Received: October 18, 2004

Ce^{3+} and Tb^{3+} coactivated $LaPO_4$ nanowires and micrometer rods were synthesized by hydrothermal methods. Their fluorescent spectra and dynamics were systematically studied and compared. The results indicated that the extinction coefficients of Ce^{3+} and Tb^{3+} in nanowires were higher than those in micrometer rods. The electronic transition rates of Ce^{3+} and Tb^{3+} in nanowires had little variation in contrast to those in micrometer rods, and the energy transfer rate and efficiency of $Ce^{3+} \rightarrow Tb^{3+}$ in nanowires were reduced greatly. It is important to observe that the brightness for the $^5D_4-{}^7F_5$ green emissions of Tb^{3+} via energy transfer of $Ce^{3+} \rightarrow Tb^{3+}$ in nanowires increased several times that in micrometer rods. This was attributed to the decreased energy loss in the excited states, being higher than $^5D_4$ due to the hindrance of the boundary.

I. Introduction

One-dimensional (1D) structures, such as tubes, wires, rods, and belts, have aroused remarkable attention over past decade due to a great deal of potential applications, such as in data storage,[1] advanced catalysts,[2] photoelectronic devices,[3] and so on. However, in comparison with zero-dimensional (0D) structures, the space anisotropy of a 1D structure provided a better model system to study the dependence of electronic transport, optical, and mechanical properties on size confinement and dimensionality.[4,5]

Rare earth (RE) compounds are intensively applied in luminescent and display devices. It is suspected that in nanosized RE compounds the luminescent quantum efficiency (QE) and display resolution could be improved.[6] Therefore, RE-doped nanosized phosphors have attracted considerable attention, for both 1D structures[7−9] and 0D nanoparticles (NPs).[10−12] Over the past several years, our research targets mainly focused on the luminescent properties, such as electronic transitions, and the surface effects for 0D NPs doped with RE compounds.[13,14] Very recently, we observed that the electronic radiative transition rate and the luminescent QE of Eu^{3+} in $LaPO_4$−Eu^{3+} nanowires (NWs) were improved nearly 2 times in comparison with NPs, which aroused our interest in 1D nanosized materials.[15]

Ce^{3+} and Tb^{3+} ions are important RE ions, which have been applied in blue and green phosphors. The energy transfer (ET) processes between Ce^{3+} and Tb^{3+} in some micrometer-sized hosts, the so-called bulk powders, such as lanthanum oxybromide,[16] aluminate,[17] alkaline earth sulfate,[18] and so on, were intensively investigated. As efficient green phosphors, Ce^{3+} and Tb^{3+} coactivated $LaPO_4$ bulk powders were extensively applied in fluorescent lamps, cathode ray tubes (CRTs), and plasma display panels (PDPs) due to the high-efficiency ET between Ce^{3+} and Tb^{3+} ions.[19,20] In 1999, Meyssamy and co-workers synthesized $LaPO_4$−Eu and $CePO_4$−Tb NPs and NWs and reported their luminescent properties.[7] Later, they reported the photoluminescence characteristics of $CePO_4$−Tb colloidal nanocrystals.[21] Kompe et al. reported luminescent enhancement in $CePO_4$−Tb/$LaPO_4$ core−shell structures.[22] To obtain efficient green phosphors of 1D $LaPO_4$−Ce^{3+}/Tb^{3+} NWs, the electronic transition and ET processes in 1D NWs should be studied and compared with the corresponding bulk powders. However, studies on ET processes between Ce^{3+} and Tb^{3+}, even between different RE impurity centers, were rather rare until now. Recently, we successfully fabricated Ce^{3+} and Tb^{3+} coactivated $LaPO_4$ NWs as well as micrometer-sized rods (MRs) by hydrothermal methods. In this paper, we study and compare their electronic transition and ET processes by luminescent spectra and dynamics.

II. Experimental Section

A. Sample Preparation. The preparation of 1D $LaPO_4$ NWs was described in detail in one of our previous papers.[15] First, appropriate amounts of high-purity La_2O_3, $Ce_2(CO_3)_3$, and Tb_4O_7 were dissolved in concentrated HNO_3, and an appropriate volume of deionized water was added. Then, an appropriate volume of $(NH_4)_2HPO_4$ aqueous solution (0.20 M) was added to the above solution. The final pH value was adjusted to 1−2 with a dilute HNO_3 solution (1 M). After being stirred well, the milky colloid solution was poured into several closed Teflon-lined autoclaves and subsequently heated at 120 °C (for NWs) and 150 °C (for MRs) for 3 h. The obtained suspension was centrifuged at 2770*g* for 15 min, and the supernatant was discarded. The resulting precipitant was washed with distilled water and dried at 50 °C under vacuum conditions.

B. Measurements. The crystal structure, morphology, and size were obtained by X-ray diffraction (XRD) using a Cu target radiation resource (λ = 1.54078 Å), transmission electron microscopy (TEM), and scanning electron microscopy (SEM) utilizing a JEM-2010 electron microscope. The excitation and emission spectra at room temperature were measured with a Hitachi F-4500 fluorescence spectrometer. In the measurements of the fluorescent dynamics of Tb^{3+}, the samples were put into a liquid-helium-cycling system, where the temperature varied from 10 to 300 K. A 355-nm light generated from a third-harmonic generator pumped by a pulsed Nd:YAG laser was used as the excitation source, with a line width of 1.0 cm^{-1}, a pulse duration of 10 ns, and a repetition frequency of 10 Hz.

* Author to whom correspondence should be addressed. Fax: 86-431-6176320. E-mail: songhongwei2000@sina.com.cn.

10.1021/jp045238e CCC: $30.25
Published on Web 05/19/2005

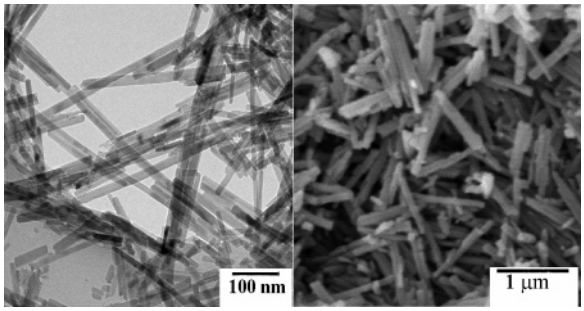

Figure 1. TEM micrograph of the NWs (left) and SEM micrograph of the MRs (right).

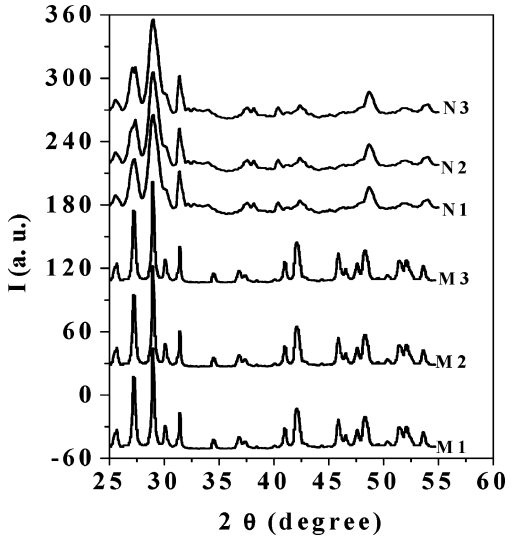

Figure 2. XRD patterns of $LaPO_4-Tb$ NWs and MRs. N1, N2, and N3 are $LaPO_4-1\%Tb$, $LaPO_4-5\%Tb$, and $LaPO_4-8\%Tb$ NWs, respectively. M1, M2, and M3 are $LaPO_4-1\%Tb$, $LaPO_4-5\%Tb$, and $LaPO_4-8\%Tb$ MRs, respectively.

The dynamics were recorded with a Spex-1403 spectrometer, a photomultiplier, and a boxcar integrator and processed by a computer. The fluorescence dynamics of Ce^{3+} were measured with a FL920 single-photon spectrometer using a nanosecond flashlamp (pulse width, 1 ns; repetition rate, 40 kHz) as the excitation source.

III. Results

A. Morphology and Structure. Figure 1 shows TEM and SEM images of $LaPO_4$ NWs and MRs. From TEM and SEM micrographs, the widths of NWs prepared at 120 °C are 10−20 nm, and the lengths are ∼0.5 μm, while the widths of MRs prepared at 150 °C are ∼200 nm and the lengths are ∼2 μm.

Figure 2 shows the XRD patterns of $LaPO_4-Tb$ samples. Like the $LaPO_4$ polycrystals prepared by the solid-state reaction, the crystal structure of both samples is of the monoclinic monazite type.[23] The relative intensities of the XRD peaks over the range of 40−55° for the NWs changed in comparison with those for the MRs, which was attributed to the shape anisotropy. It should be pointed out that in Tb-doped, Ce-doped, or Ce/Tb-codoped samples no additional phase was observed.

B. Excitation and Emission Spectra. Figure 3 shows the excitation and emission spectra in Ce^{3+}-activated $LaPO_4$ powders. It can be seen that the excitation bands consist of three components, having peaks at 241, 258, and 276 nm, respectively. These peaks are associated with allowed f−d transitions from the ground-state $^2F_{5/2}$ to different crystal-field components of the 5d level. The emission band consists of two peaks with

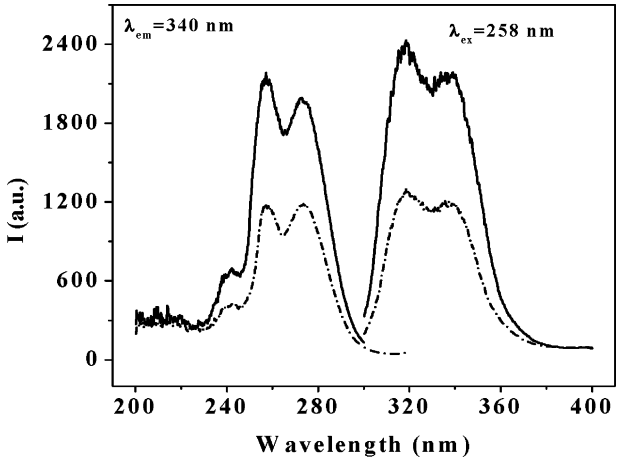

Figure 3. Excitation (left) and emission spectra (right) of Ce^{3+} in $LaPO_4-1\%Ce$ powders. Solid lines and dashed−dotted lines represent the MRs and NWs, respectively.

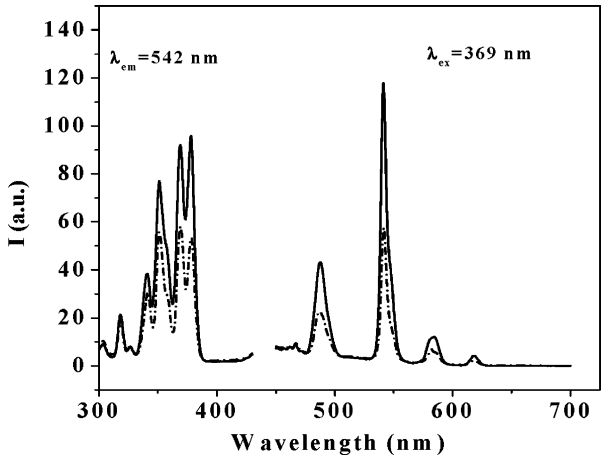

Figure 4. Excitation (left) and emission spectra (right) of Tb^{3+} in $LaPO_4-2.5\%Tb$ powders. Solid lines and dashed−dotted lines represent the MRs and NWs, respectively.

maxima at 318 and 340 nm, corresponding to the transitions from the lowest 5d excited state to the spin−orbit components (^2D) of the doublet ground state, $^2F_{5/2}$ and $^2F_{7/2}$. The energy difference between the two emission maxima is ∼ 2034 cm^{-1}, which is basically in accordance with the energy difference obtained by theory between the spin−orbit split $^2F_{5/2}$ and $^2F_{7/2}$ doublets (about 2000 cm^{-1}). The results above were similar to those of the bulk $LaPO_4-Ce^{3+}$ samples.[24]

Figure 4 shows the excitation and emission spectra in Tb^{3+}-activated $LaPO_4$ powders. Many excitation lines of Tb^{3+} ions exist in the UV range, which were associated with $^7F_6 - {}^5D_3$, $^7F_6 - {}^5G_J$, and $^7F_6 - {}^5L_6$ transitions of Tb^{3+}, while the emission lines from 480 to 650 nm were associated with the $^5D_4-{}^7F_J$ ($J = 3-6$) transitions. Among them, the green $^5D_4-{}^7F_5$ emission at 542 nm was the strongest.

Figure 5 shows the excitation spectra in Ce^{3+}/Tb^{3+}-coactivated $LaPO_4$ powders. As the emission of Tb^{3+} at 542 nm was monitored, the stronger allowed f−d transitions of Ce^{3+} and the weaker forbidden f−f transitions of the Tb^{3+} ions were observed, implying efficient ET from Ce^{3+} to Tb^{3+} ions. It is clear that the intensity of the Tb^{3+} transition originating from the $Ce^{3+}-Tb^{3+}$ ET excitation is 2 orders higher than that from the f−f transitions of Tb^{3+}. Because the f−f transitions of the Tb^{3+} ions are electronic dipole forbidden ones, the excitation efficiency for Tb^{3+} itself is very low. However, the luminescent intensity can be dramatically increased through exciting Ce^{3+}

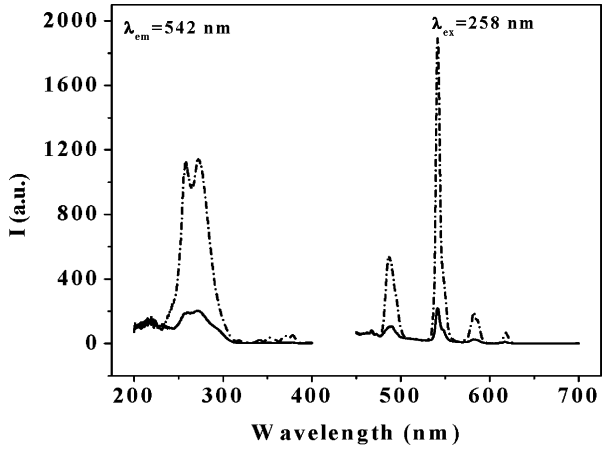

Figure 5. Excitation (left) and emission spectra (right) for $LaPO_4$−1%Ce/2.5%Tb samples. Solid lines and dashed−dotted lines represent the MRs and NWs, respectively.

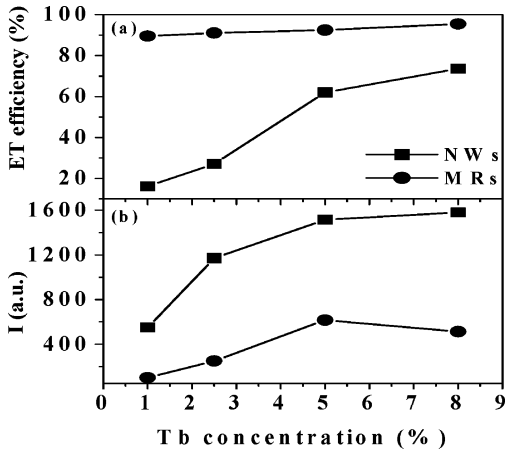

Figure 6. (a) Dependence of ET efficiency and (b) emission intensity of Tb^{3+} at 258 nm excitation on the Tb^{3+} concentration for the same Ce^{3+} concentration (1%).

ions in Ce^{3+}/Tb^{3+}-coactivated $LaPO_4$ NWs, similar to that in the bulk materials.

From Figures 3−5, it can be seen that in Tb^{3+}-doped or Ce^{3+}-doped powders the emission intensity for Tb^{3+} or Ce^{3+} in NWs is a bit lower than that in MRs. However, in Ce^{3+}/Tb^{3+}-codoped powders, the emission intensity for Tb^{3+} in NWs through ET excitation is much higher than that in MRs. In the following section, its origin will be discussed.

C. ET Efficiency and Emission Intensity on Ce^{3+} Concentration. Figures 6a and 6b show, respectively, the dependence of the ET efficiency of $Ce^{3+}-Tb^{3+}$ and the $^5D_4-^7F_5$ emission intensity on the Tb^{3+} concentration in $LaPO_4-Ce^{3+}/Tb^{3+}$ powders. The ET efficiency from a donor (Ce^{3+}) to an acceptor (Tb^{3+}) was calculated according to the formula $\eta_{ET} = 1 - I_d/I_{d0}$, where I_d and I_{d0} were the corresponding luminescence donor intensities in the presence and absence of the acceptor for the same donor concentration, respectively. It can be seen that the ET efficiency for both NWs and MRs increased with Tb^{3+} concentration and that in the NWs increased more rapidly. The ET efficiency in the NWs was lower than that in the MRs for any Tb^{3+} concentration. The intensities of the $^5D_4-^7F_5$ transitions in the NWs are 3−5 times higher than those in the MRs. As the Tb^{3+} concentration increased from 1% to 5%, the emission intensity in the MRs increased. As Tb^{3+} concentration increased continuously, the emission intensity decreased. This means that the fluorescence quenching concentration in the MRs is around 5%. The emission intensity in the NWs increased all

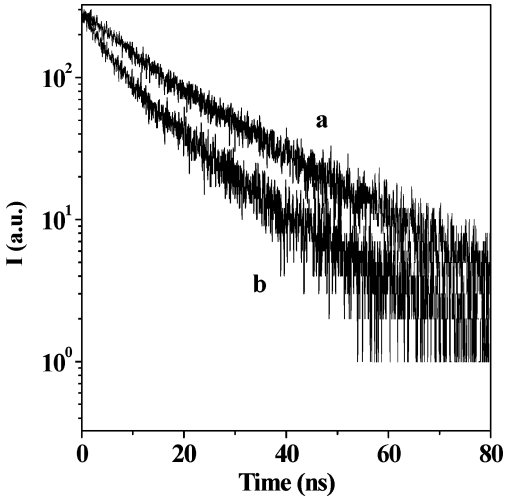

Figure 7. Typical fluorescence decay curves in Ce^{3+}-doped and Ce^{3+}/Tb^{3+}-codoped $LaPO_4$ MRs: (a) $LaPO_4$−1%Ce; (b) $LaPO_4$−1%Ce/5%Tb.

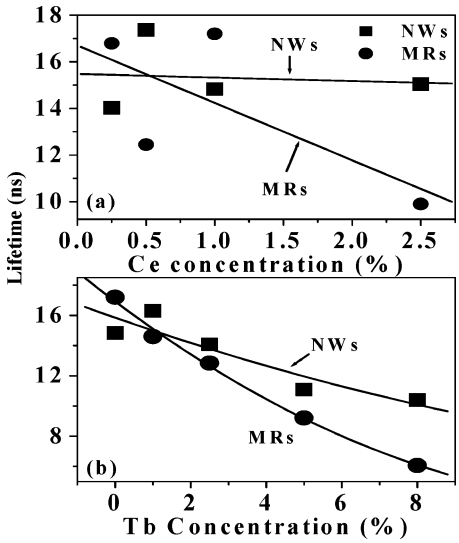

Figure 8. Dependence of Ce^{3+} lifetime (a) on the Ce^{3+} concentration for singly doped Ce^{3+} samples and (b) on the Tb^{3+} concentration for the same Ce^{3+} content (1%). Scattered points are the experimental data, and the solid lines are the fitted curves.

of the time as the Tb^{3+} concentration varied from 1% to 8%, indicating that the quenching concentration is higher than 8%. The results above show that the quenching concentration in the NWs was higher than that in the MRs.

D. Luminescent Dynamics of Ce^{3+}. The luminescent dynamics of Ce^{3+} at room temperature in the NWs and MRs were measured and compared. Figure 7 shows the typical luminescent dynamics of Ce^{3+} in $LaPO_4-Ce^{3+}/Tb^{3+}$. It can be seen that in the Ce^{3+}-doped sample the fluorescence decays strictly obey the exponential rule. In the Ce^{3+}/Tb^{3+}-codoped sample, the fluorescence decaysdeviate a little from the exponential rule due to the ET of $Ce^{3+} \rightarrow Tb^{3+}$, and the decay time constant becomes shorter.

Figure 8 shows the dependence of the exponential lifetime of the 5d−4f transitions for Ce^{3+} on the Ce^{3+} and Tb^{3+} concentrations. In Figure 8a, as the concentration of Ce^{3+} varied from 0.25% to 2.5%, the lifetime in the NWs hardly changed, indicating that the quenching concentration can be neglected. In the MRs, as the Ce^{3+} concentration varied from 0.25% to 2.5%, the lifetimes decreased. This indicates that the fluorescence quenching concentration of Ce^{3+} in the NWs was higher

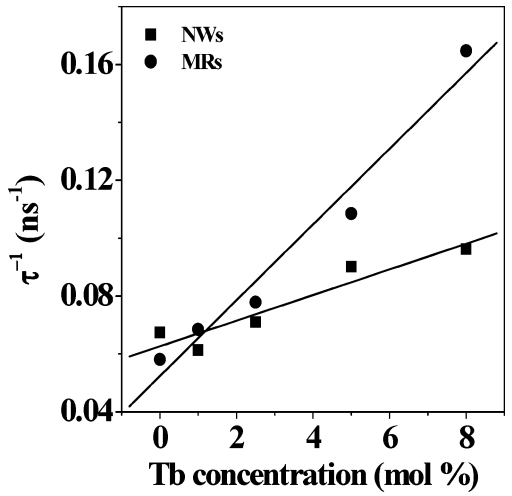

Figure 9. Dependence of τ^{-1} on Tb^{3+} concentration. Scattered points are the experimental data, and the solid lines are the fitted curves.

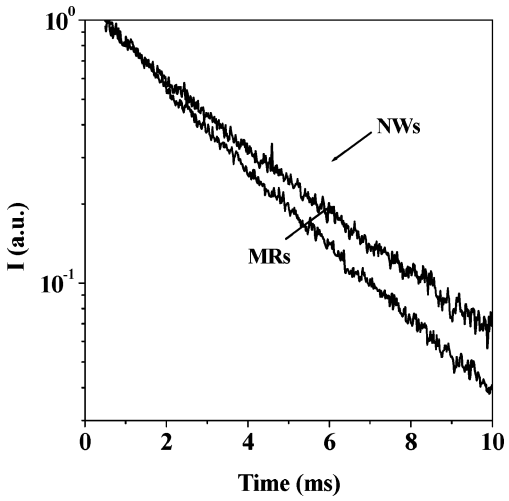

Figure 10. Decay curves of the $^5D_4$ level of Tb^{3+} in $LaPO_4$−2.5%Tb NWs and MRs.

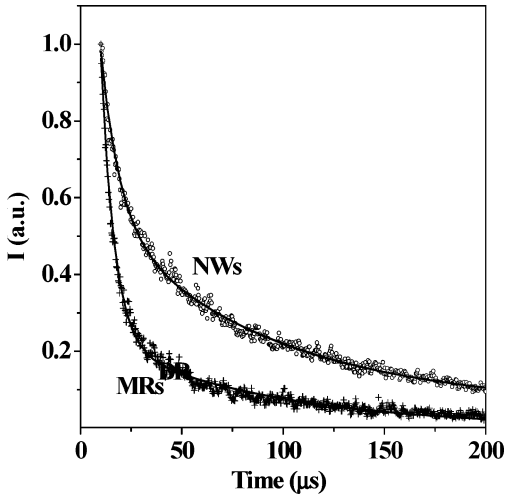

Figure 11. Fluorescence decay curves of $^5D_3-^7F_5$ in $LaPO_4$−2.5%Tb NWs and MRs.

than that in the MRs, similar to the quenching concentration of Tb^{3+}. In Figure 8b, the lifetime of Ce^{3+} in both the NWs and the MRs decreased with the concentration of Tb^{3+}, and in the MRs it decreased more rapidly.

In Ce^{3+}-doped samples, the reciprocal of the fluorescence lifetime equals the electronic transition rate (including the radiative and nonradiative transitions). In Ce^{3+}/Tb^{3+}-codoped samples, the reciprocal of the fluorescence lifetime equals the sum of the electronic transition rate of Ce^{3+} and the ET rate of $Ce^{3+} \rightarrow Tb^{3+}$. Figure 9 shows the reciprocal of the fluorescence lifetime of Ce^{3+} versus Tb^{3+} concentration. It can be seen that the reciprocal of the fluorescence lifetime increased linearly with the increase in Tb^{3+} concentration. Therefore, the experimental points were fitted with the following function

$$\tau^{-1} \propto R_C + R_{ET}[Tb^{3+}] \quad (1)$$

where R_C is the total electronic transition rate of Ce^{3+}, including the radiative and nonradiative transitions, R_{ET} is the average ET rate of $Ce^{3+} \rightarrow Tb^{3+}$, and $[Tb^{3+}]$ is the concentration of Tb^{3+}. By fitting, R_C was deduced to be 6.3×10^{-2} ns^{-1} in the NWs and 5.2×10^{-2} ns^{-1} in the MRs. R_{ET} was deduced to be 0.44 ns^{-1} mol^{-1} in the NWs and 1.30 ns^{-1} mol^{-1} in the MRs. The electronic transition rate of Ce^{3+} in the NWs increased a little more than that in the MRs, while the ET rate of $Ce^{3+} \rightarrow Tb^{3+}$ in the NWs decreased nearly 3 times.

E. Luminescent Dynamics of Tb^{3+}. The fluorescence dynamics for Tb^{3+} were also studied and compared. Figure 10 shows fluorescence decay curves of the $^5D_4-^7F_5$ transitions for Tb^{3+} in $LaPO_4$−Tb NWs and MRs at 10 K. It can be seen that the $^5D_4-^7F_5$ emissions decayed exponentially, for both NWs and MRs. The exponential lifetime was determined to be 2.72 ms in the NWs and 2.57 ms in the MRs. The slight variation indicated that the total electronic transition rate of $^5D_4$ hardly changed in the NWs and MRs. To determine the radiative and nonradiative transition rates, the lifetime of the $^5D_4-^7F_5$ line at different temperatures was measured. The lifetime hardly changed as the temperature varied, for both NWs and MRs. For example, the lifetime in the NWs was determined to be 2.72 ms at 10 K, 2.77 ms at 150 K, and 2.82 ms at 300 K. As it is well-known, the radiative transition rate is nearly independent of the temperature, and the nonradiative transition rate strongly depends on temperature. Therefore, the nonradiative transition rate for the $^5D_4$ state can be neglected. The reciprocal of the lifetime equals the radiative transition rate of $^5D_4 \rightarrow \Sigma^7F_J$, determined to be 0.37 ms^{-1} in the NWs and 0.39 ms^{-1} in the MRs. Actually, $^5D_4$ is the lowest excited state, and the energy separation between $^5D_4$ and the nearest lower level $^7F_0$ is as high as ~15 000 cm^{-1}. In this case, nonradiative relaxation processes hardly happen according to the theory of multiphoton relaxation.

The fluorescence dynamics of the $^5D_3-^7F_5$ transitions in the NWs and MRs were measured and compared, as shown in Figure 11. As can be seen, the decay curves included two components, a faster one and a slower one, for both NWs and MRs. They were well fitted by a biexponential function, $I = I_1 \exp(\tau_1/t) + I_2 \exp(\tau_2/t)$, with $I_1 + I_2 = 1$. The fitting parameters are $I_1 = 0.23$, $\tau_1 = 7.3$ μs, $I_2 = 0.77$, and $\tau_2 = 68$ μs for the NWs and $I_1 = 0.62$, $\tau_1 = 6.8$ μs, $I_2 = 0.38$, and $\tau_2 = 84$ μs for the MRs. The decay constants of the two components for the NWs and MRs did not change much. However, the proportions of the two components changed greatly. In the NWs the slower component is dominant, while in the MRs the faster component is dominant.

IV. Discussions

A. Concentration Quenching. In $LaPO_4-Ce^{3+}$ and $LaPO_4-Tb^{3+}$ NWs, the fluorescence quenching concentrations both increased relative to the corresponding MRs. Similar results were also reported in RE-doped NPs by several authors.[25,26] The

growth of the quenching concentration in the NWs should be similar to the increase of the quenching concentration in the NPs. Due to the defects produced during the preparation process and trace impurities contained in the raw materials, the samples inevitably have quenching centers (traps) with low concentrations. When an excited luminescent center is nearby a trap, the excited energy could be transferred easily to the trap from which it lost nonradiatively. The energy on an excited luminescent center can also be transferred to unexcited luminescent centers if these luminescent centers are close enough such that they could be coupled together by some interaction. In normal samples, when the concentration of the luminescent centers is small, most of the luminescent centers can be thought of as "isolated", and only a few luminescent centers having traps nearby will give their energy to the traps. Consequently, the luminescence quenching is not obvious. As the concentration of the luminescent centers increases, some luminescent centers may be near enough to the quenching centers, which may result in a much faster ET rate than the radiative transition rate, leading to the quenching of the luminescence. However, the luminescent centers may be near enough to form a resonant ET pair in the crystal, such that energy can be easily transferred from one luminescent center to another. If the luminescent centers are close to the quenching centers, the energy will be finally quenched. As the concentration of luminescent centers is high enough, the energy on most of the excited luminescent centers will finally transfer to traps before it is emitted via a radiative transition, leading to the concentration-dependent quenching.

In nanosized materials, due to the limited number of primitive cells per particle, on average there are only a few traps in one particle, so the traps distribute randomly with a considerably larger fluctuation among the particles. Some particles may contain many traps while others may contain no trap at all. The energy of a luminescence center can only be transferred resonantly within one particle since the ET is hindered by the particle boundary. Therefore, quenching occurs at higher a concentration in nanosized materials than in normal materials. In addition, in nanosized particles, the total internal quenching defects may decrease.

B. ET Processes. In the ET system containing donors (Ce^{3+}) and acceptors (Tb^{3+}), under the excitation of a pulsed laser, if P_i denotes the probability of the ith luminescence center being in the excited state at time t, then $P_i(t)$ varies as[27]

$$\frac{dP_i(t)}{dt} = -\gamma P_i(t) - \sum_{i,i'\neq i}^{N_D} W_{ii'}P_i(t) + \sum_{i,i'\neq i}^{N_D} P_i(t) - \sum_{j}^{N_A} X_{ij}P_i(t) \quad (2)$$

where γ is the radiative decay rate of the excited luminescent centers, $W_{ii'}$ is the ET rate from the ith to i'th luminescent center, X_{ij} is the ET rate to acceptors near the ith luminescent center, and N_D and N_A are the total numbers of donors and acceptors, respectively. The luminescent intensity at time t, $F(t)$, can be written as

$$F(t) \equiv \sum_{i}^{N_p} P_i(t) = \exp[-\gamma t - \int_0^t \langle X(t)\rangle \, dt] \quad (3)$$

with

$$\langle X(t)\rangle = \frac{\sum_{i,j}^{N_D,N_A} X_{ij}P_i(t)}{\sum_{i}^{N_D} P_i(t)} \quad (4)$$

Due to the fact that $\langle X(t)\rangle$ depends on time, the luminescent decay curve in the ET system deviates from an exponential function. Generally, the fluorescence decays faster in the original period and then becomes slower gradually. The acceptors become less and less available with increasing excitation time because some of them have been filled. In our experiments for the dynamics of Ce^{3+}/Tb^{3+}-codoped $LaPO_4$ NWs and MRs, the luminescent decay time of Ce^{3+} nearly reaches a constant with increasing time, indicating that the the filled acceptors (excited Tb^{3+}) are much less prevalent than the unfilled acceptors (ground-state Tb^{3+}) near the excited luminescent centers (Ce^{3+}).

C. Energy Loss in Excited States and Brightness for Tb^{3+}. It is interesting to observe that in Ce^{3+}/Tb^{3+}-codoped $LaPO_4$ NWs the brightness of the green emissions of $^5D_4-{}^7F_5$ was stronger than that in the MRs for the same concentrations of Ce^{3+} and Tb^{3+}. Actually, the brightness of Tb^{3+} via ET excitation was dominated by the following factors in Ce^{3+}/Tb^{3+}-coactivated materials: (1) the electronic transition rate and the concentration of Ce^{3+}, (2) the ET efficiency and rate of $Ce^{3+} \rightarrow Tb^{3+}$, (3) the relaxation processes from higher excited states of Tb^{3+} to the $^5D_4$ states, and (4) the electronic transition rate and concentration of Tb^{3+}. In the above sections, we have discussed these processes separately. We can assume that in the NWs and MRs prepared by the same method the concentrations for Tb^{3+}/Ce^{3+} have little variation. In $LaPO_4-Eu$, we measured the practical concentration of europium in the NWs and MRs and observed that the practical concentrations for the NWs (4.16% in mol) and MRs (4.23% in mol) were nearly same and close to the starting concentrations of the samples (5% in mol). The doping of Ce^{3+} or Tb^{3+} should be similar. Because the electronic transition rate for Ce^{3+} or Tb^{3+} in the NWs and MRs had little variation, the ET rate of $Ce^{3+} \rightarrow Tb^{3+}$ in the NWs decreased 3 times more than that in the MRs and the concentration variation of Ce^{3+} and Tb^{3+} ions in the NWs and MRs was negligible, the brightness for the $^5D_4-{}^7F_J$ emissions in the NWs should be lower than that in the MRs if the nonradiative relaxation processes were not considered. Surprisingly, the brightness in the NWs is higher than that in the MRs. Therefore, we have to reconsider the nonradiative relaxation processes.

In $LaPO_4-Ce^{3+}/Tb^{3+}$ with exciting Ce^{3+} ions, electrons were excited from the ground state, $^2F_{5/2}$, to the 5d excited state of Ce^{3+} and then to some excited states of Tb^{3+}. The electrons at higher excited states relax to $^5D_4$ and generate the $^5D_4-{}^7F_5$ transitions. According to the energy levels of Ce^{3+} and Tb^{3+} and the Foster−Dexter theory, the ET from Ce^{3+} to the $^3H_6$ level of Tb^{3+} has the largest probability.[28,29] On one hand, the electrons in the higher excited states can nonradiatively relax to the lower excited states. On the other hand, if some defect states exist near Tb^{3+}, then the energies of the higher excited-state electrons can transfer to the defect states and electrons nonradiatively transit to the ground states, as shown in Figure 12, the schematic of the ET and luminescent processes of $LaPO_4-Ce^{3+}/Tb^{3+}$. If the ET processes from Tb^{3+} to the defect levels happen, then the populations of luminescent Tb^{3+} ions will decrease. The fluorescent dynamics of the $^5D_3-{}^7F_5$ transitions strongly support our assumption. It was proposed that the

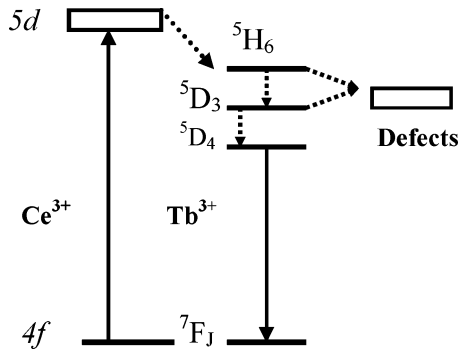

Figure 12. Schematic for the ET and luminescence processes in Ce^{3+}/Tb^{3+}-codoped $LaPO_4$ NWs and MRs.

two components for the $^5D_3-^7F_5$ transitions corresponded to two processes, the slower one to the nonradiative relaxation of $^5D_3-^5D_4$ and the faster one to the ET from $^5D_3$ to some defect levels, because the nonradiative ET rate between the luminescent center of a RE compound and a defect level nearby is much faster than the nonradiative relaxation rate of a RE compound.[30,31] In the MRs, although more Tb^{3+} ions are excited to excited states through the ET of $Ce^{3+} \rightarrow Tb^{3+}$, most of them nonradiatively transit to the ground state again through the ET of Tb^{3+} to the defect levels. In the NWs, despite the fact that fewere Tb^{3+} ions are excited to excited states, most of them generate $^5D_4-^7F_J$ emissions because the ET processes of the $Tb^{3+} \rightarrow$ defect levels in higher excited states decreased. Therefore, the brightness for the green emissions of Tb^{3+} in the NWs increased. However, we cannot identify the defect states in $LaPO_4-Ce^{3+}/Tb^{3+}$.

V. Conclusions

The $LaPO_4-Ce/Tb$ NWs and the corresponding MRs were fabricated by hydrothermal methods, and their photoluminescent properties were compared with each other. The results indicate that the electronic transition rates of $5d-^2F_{5/2}/^2F_{7/2}$ transitions for Ce^{3+} and the $^5D_4-^7F_J$ transitions for Tb^{3+} had little variation in the two different samples, NWs and MRs. From MRs to NWs, the ET rate of $Ce^{3+}-Tb^{3+}$decreased from 1.3 to 0.44 ns^{-1} mol^{-1}, and the ET efficiency also decreased. However, in Ce^{3+}/Tb^{3+}-coactivated NWs, the brightness for the green emissions of $^5D_4-^7F_J$ transition was improved more than that in the MRs. The fluorescence dynamics of the $^5D_3-^7F_5$ transition indicate that besides the nonradiative transition of $^5D_3-^5D_4$ the ET process of $Tb^{3+} \rightarrow$ defects probably exists. The amount of this process in the NWs is much smaller than that in the MRs, leading to the decreased energy loss from the level higher than $^5D_4$ and the increased luminescent QE of $^5D_4-^7F_J$. This can be also attributed to the hindrance of the boundary.

Acknowledgment. We are grateful for the financial support of the One-Hundred Project from the Chinese Academy of Sciences and the National Natural Science Foundation of China (Grant Nos. 10374086 and 10274083).

References and Notes

(1) Kong, Y.; Yu, D.; Zhang, B.; Fang, W.; Feng, S. *Appl. Phys. Lett.* **2001**, *78*, 4.
(2) Daun, X.; Yang, Y.; Cui, Y.; Wang, J.; Lieber, C. *Nature* **2001**, *409*, 66.
(3) Pan, Z.; Dai, Z.; Wang, Z. *Science* **2001**, *291*, 1947.
(4) Huang, M.; Mao, S.; Feick, H.; Yan, H.; Wu, Y.; Kind, H.; Weber, E.; Russo, R.; Yang, P. *Science* **2001**, *292*, 1897.
(5) Xia, Y.; Yang, P. *Adv. Mater.* **2003**, *15*, 351.
(6) Bhargava, R.; Gallagher, D.; Hong, X. *Phys. Rev. Lett.* **1994**, *72*, 416.
(7) Meyssamy, H.; Riwotzki, K. *Adv. Mater.* **1999**, *11*, 840.
(8) Yada, M.; Mihara, M.; Mouri, S.; Kijima, T. *Adv. Mater.* **2002**, *14*, 309.
(9) Wang, X.; Li, Y. *J. Eur. Chem.* **2003**, *9*, 5627.
(10) Meltzer, R. S.; Feofilov, S. P.; Tissue, B. *Phys. Rev. B* **1999**, *60*, R14012.
(11) Williams, D. K.; Bihari, B.; Tissue, B. M.; McHale, J. M. *J. Phys. Chem. B* **1998**, *102*, 916.
(12) Song, H.; Chen, B.; Peng, H.; Zhang, J. *Appl. Phys. Lett.* **2002**, *81*, 1776.
(13) Song, H.; Wang, J.; Chen, B.; Lu, S. *Chem. Phys. Lett.* **2003**, *376*, 1.
(14) Peng, H.; Song, H.; Chen, B.; Wang, J.; Lu, S.; Kong, X.; Zhang, J. *J. Chem. Phys.* **2003**, *118*, 3277.
(15) Song, H.; Yu, L.; Lu, S.; Wang, T.; Liu, Z.; Yang, L. *Appl. Phys. Lett.* **2004**, *85*, 470.
(16) Holsa, J.; Leskela, M.; Niinisto, L. *J. Solid State Chem.* **1981**, *37*, 267.
(17) Jia, D.; Jia, W.; Wang, X.; Yen, W. *Solid State Commun.* **2004**, *129*, 1.
(18) Jose, M.; Lakshmanan, A. *Opt. Mater.* **2004**, *24*, 651.
(19) Dexpert-Ghys, J.; Mauricot, R.; Faucher, M. D. *J. Lumin.* **1996**, *69*, 203.
(20) Wu, X.; You, H.; Gui, H.; Zeng, X.; Hong, G.; Kim, C.; Pyun, C.; Yu, B.; Park, C. *Mater. Res. Bull.* **2002**, *37*, 2531.
(21) Riwotzki, K.; Meyssamy, H.; Kornowski, A.; Haase, M. *J. Phys. Chem. B* **2000**, *104*, 2824.
(22) Kompe, K.; Borchert, H.; Storz, J.; Lobo, A.; Adam, S.; Moller, T.; Haase, M. *Angew. Chem., Int. Ed.* **2003**, *42*, 5513.
(23) Rambabu, U.; Buddhudu, S. *Opt. Mater.* **2001**, *17*, 401.
(24) Yu, M.; Lin, J.; Fu, J.; Han, Y. C. *Chem. Phys. Lett.* **2003**, *371*, 178.
(25) Wei, Z.; Sun, L.; Liao, C.; Yin, J.; Jiang, X.; Yan, C. *J. Phys. Chem. B* **2002**, *106*, 10610.
(26) Huignard, A.; Gacoin, T.; Pierre, J. *Chem. Mater.* **2000**, *12*, 1090.
(27) Huber, D. In *Laser Spectroscopy of Solids*; Yen, W. M., Selzer, P. M., Eds.; Springer: Berlin, 1981; p 83.
(28) Foster, T. *Z. Naturforsch., A: Phys. Sci.* **1949**, *4*, 321.
(29) Dexter, D. *J. Chem. Phys.* **1953**, *21*, 836.
(30) Huang, S.; Lou, L. *J. Lumin.* **1990**, *45*, 377.
(31) Lou, L.; Huang, S. *J. Lumin.* **1988**, *40/41*, 667.